Fast-Response Aircraft Temperature Sensors

CARL A. FRIEHE AND DJAMAL KHELIF

Department of Mechanical and Aerospace Engineering, University of California, Irvine, California

(Manuscript received 21 October 1991, in final form 13 April 1992)

ABSTRACT

Three aircraft temperature sensors were compared in clear-air conditions on the NCAR King Air: a standard Rosemount nondeiced, fast-response flight test probe, the NCAR K probe, and a modified Rosemount probe with the platinum wire element replaced with a small thermistor bead. Responses to transient temperature changes were compared from soundings through sharp inversions. High-frequency spectral comparisons were obtained from level runs in the marine boundary layer. All three probes followed a two-time-constant response. The response of the thermistor-modified Rosemount probe was, however, much closer to a one-time-constant model than the two others. Following previous results and analyses, it appears that the longer time constant in the Rosemount probe is largely due to the contact of the platinum wire element, which is wound around mica supports. The long unsupported wire elements in the NCAR K probe do produce a superior high-frequency response, but low-frequency response is anomalous, perhaps due to the large plastic body placed upstream of the wires to separate out particles. The two-time-constant temperature response was compared for the three probes by developing expressions for the time derivative and time integral of the normalized temperature that separated the relative contributions of the sensor element and its support.

1. Introduction

Fast-response aircraft air-temperature sensors are required for many applications: direct measurement of turbulent heat flux, temperature spectra, calculation of true airspeed, and accurate measurement of transients, such as inversions. The standard sensor has been the Rosemount[1] total air-temperature probe, which is characterized by a reasonably high recovery factor[2] (0.95–0.98) and also provides for some separation of liquid water in clouds to keep the platinum wire element dry. These attributes are due to the unique design of the housing, which both slows the air almost adiabatically and inertially separates out a reasonably large fraction (the exact amount is unknown) of the liquid water droplets (Fig. 1a) in rain. The housing is also designed to bleed off internal boundary layers, so that the air reaching the sensor has minimal contact with the housing surfaces.

Early in the use of the Rosemount probe with the smallest temperature element [25-μm-diameter (d) platinum wire] for meteorological studies, it became apparent that the probe had two time constants. Rosemount (1963) attributes the shorter time constant to the wire itself and the longer time constant to the combined effects of the housing, sensor shield, and sensor supports. Rodi and Spyers-Duran (1972) and McCarthy (1973a) examined the time response from in-flight data in terms of the two-time-constant model. Acheson (1973) criticized McCarthy's approach as having no physical basis; McCarthy (1973b) responded that the two time constants determined empirically from in-flight data appeared to adequately describe the response. Lenschow (1972) examined the response of the Rosemount probe and explained that the longer time constant is associated with the supporting structure of the wire. He also presented in-flight data comparing the Rosemount probe and an unprotected wire that showed the slowness of the Rosemount response in attaining a final temperature due to the longer time constant. Since then, the approaches to the measurement of fast temperature have been to use the Rosemount probe, and perhaps correct it for the two-time response, as Ritter et al. (1987) have done, or develop new sensors, as NCAR (see Spyers-Duran and Baumgardner 1983) and Lawson (1991) have done. These new sensors are characterized, however, by low recovery factors of about 0.8. This is of some concern, as Wyngaard (1988) has shown that low-recovery-factor temperature probes can give erroneous fluctuating air-temperature measurements when used in regions of high flow distortion, such as around an aircraft fuselage.

[1] Rosemount Engineering Company, Eagan, Minnesota.

[2] The recovery factor is the fraction of the free-stream kinetic energy that is isentropically recovered as thermal energy in the fluid adjacent to the sensor.

Corresponding author address: Dr. Carl A. Friehe, Department of Mechanical Engineering, University of California, Irvine, CA 92717.

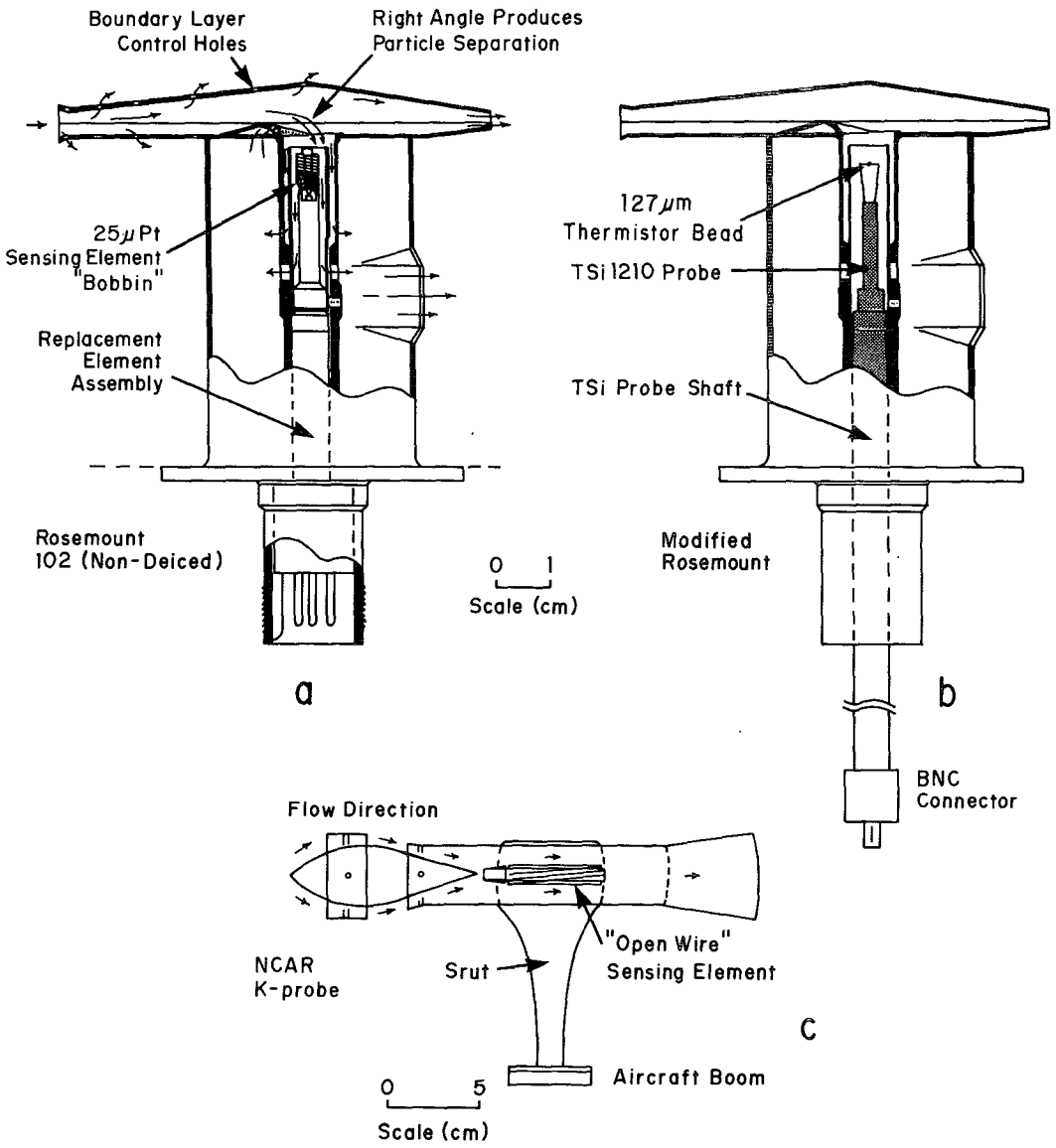

FIG. 1. (a) Cross-sectional view of Rosemount 102 nondeiced total air-temperature sensor (reproduced with permission of Rosemount Engineering Corporation). (b) Cross-sectional view of modified Rosemount sensor. (c) Cross-sectional view of NCAR K probe.

Therefore, it seems desirable to stay with the proven Rosemount design as much as possible because of the high recovery factor, but attempt to reduce the longer, second time constant. We believe that this is possible because, following Lenschow's analysis, if the undesirably long time constant of the Rosemount probe is due primarily to the internal mounting of the platinum resistance wire inside the housing, it could possibly be eliminated or reduced by using a different sensing element. In order to achieve a nominal resistance of 50 Ω of 25-μm-diameter platinum wire inside the housing, Rosemount winds the wire around four mica supports in a compact helix, with about $l = 3.6$ mm of wire suspended between supports (see Fig. 1a). This results in the platinum wire contacting a mica support about every 145 wire diameters. Lenschow (1972) and Paranthoen et al. (1982) have shown that such small l/d ratios give an unwanted second, longer time constant due to the conduction along the wire to the supports, which causes the measured temperature to lag the true ambient temperature. For measurements to be unaffected by supports, the l/d of the resistance wire should be at least 1000, preferably 2000, according to Paranthoen et al. This is not possible for the 25-μm wire in the small space in the present housing. In the present study, we simply replaced the platinum element by a single small thermistor bead in order to minimize the second time constant.

TABLE 1. Measured parameters of different platinum wire sensors.

Sensor	U_∞ (m s^{-1})	d (μm)	Re*	A_s	τ_s (s)	τ_h (s)	Source
Rosemount 102E4AL	58.0	25	30.2	0.70	0.016	1.15	Manufacturer
Rosemount 102E4AL	80.0	25	41.7	0.70	0.045	0.17	**
NCAR K probe	80.0	25	41.7	1.0	0.040	0.00	**
NCAR K probe	80.0	12.5	20.8	1.0	0.036	0.00	**

* The Reynolds number is calculated using $0.3U_\infty$, which we assume to be the airspeed inside the housing.
** Spyers-Duran and Baumgardner (1983).

2. Sensors

The modification of the Rosemount 102E4AL temperature probe was straightforward: the internal resistance wire element subassembly was removed and replaced with a similar subassembly with a 127-μm thermistor,[3] as shown in Fig. 1b. For ease of installation, mounting, and replacement of the thermistor, a TSI (St. Paul, Minnesota) hot-wire anemometer probe (model 1210) was used that consists of two gold-plated stainless steel needles about 1.5 mm apart, across which the 18-μm-diameter thermistor bead wires were soldered. Thus, the thermistor bead is supported by wires of $l/d = 40$ on each side. The heat conduction from the thermistor bead through the mounting wires to the needles is unknown, but presumed small. The TSI probe plugs into a TSI support shaft that allows easy removal of the probe for repair or cleaning. We replicated the brass shield of the Rosemount subassembly around the TSI probe support, as this must be an integral part of the flow control inside the housing. The recovery factor of this modified Rosemount probe was found to be the same as that for the regular Rosemount sensor from in-flight speed run data.

A dc–Wheatstone bridge circuit was used with the nominal 5-KΩ thermistor. The output voltage was slightly nonlinear with temperature, due to the exponential response of the thermistor to temperature. The thermistor and bridge combination was calibrated in a constant-temperature bath of deionized water. The nonlinear calibration was used in the data reduction.

The NCAR K probe, shown in Fig. 1c, is an open-wire temperature sensor using a 25-μm-diameter platinum wire, with l/d approximately 2000 between supports. The wire is installed almost parallel to the direction of the airflow. The sensing element is shielded against particles and hydrometeors by a plastic bulb placed upstream. The recovery factor of this probe is about 0.8 (P. Spyers-Duran, personal communication, 1991).

The modified sensor, along with a standard Rosemount 102E4AL and an NCAR K probe, were mounted circumferentially on the NCAR King Air 0.64 m behind the tip of the radome gust probe [Brown et al. (1983)]. The data were recorded at 50 Hz with a 14-bit analog-to-digital convertor and antialiasing filters at 10 Hz and processed at NCAR to a final rate of 20 Hz. The resolution is about 0.06°C for all three probes.

[3] BB05, Thermometrics Inc., Edison, New Jersey.

3. Time constants

The time constant of a resistance temperature sensor is governed by the heat transfer between the sensing element and the surrounding fluid. Although the heat-transfer formulas are reasonably well known (Sandborn 1972; La Rue et al. 1975), results from experimental in situ measurements of the time constants of aircraft sensors vary widely. A compilation of some of those results is given in Table 1. In all of these studies the sensing elements were platinum wires. The measurements in the first table entry were made in a wind tunnel, whereas the three others were obtained from an aircraft flying at 2740 m.

To analyze the transient response of both types of sensors it will be assumed that only forced convection takes place in the heat-transfer process and that there are no axial or radial temperature gradients. The heat-transfer rate between the sensing element and the air is expressed as

$$\dot{Q} = -\bar{h}A_s(T_s - T_\infty), \tag{1}$$

where $\dot{Q}$ is the heat-transfer rate, A_s is the surface area of the sensing element in contact with the air, T_s is the mean temperature of the sensor, and T_∞ is the free-stream air temperature. The mean heat-transfer coefficient $\bar{h}$ is a function of the airspeed and physical properties of the air that are expressed through the Reynolds and Prandtl numbers.

The heat-transfer rate $\dot{Q}$ is related to the change in internal energy of the sensor by

$$\dot{Q} = \frac{dU}{dt}, \tag{2}$$

where

$$U = \rho_s c_s V_s (T_s - T_{\text{ref}}), \tag{3}$$

and U is the internal thermal energy, V_s is the volume of the sensing element, ρ_s its density, and c_s its thermal heat capacity. Here T_{ref} is a constant reference temperature at which $U \equiv 0$. Assuming that T_∞ is constant, and after combination of (1), (2), and (3) and rear-

rangement, the differential equation for the thermal response is obtained:

$$\frac{d(T_s - T_\infty)}{T_s - T_\infty} = -\frac{\bar{h}A_s}{\rho_s c_s V_s}\,dt. \tag{4}$$

If T_0 is the initial temperature of the sensor ($t = 0$, $T_s = T_0$), the solution of this equation is

$$\Theta = \frac{T_s - T_\infty}{T_0 - T_\infty} = e^{-t/\tau_s}, \tag{5}$$

where

$$\tau_s = \frac{\rho_s c_s V_s}{\bar{h}A_s} \tag{6}$$

and is the time constant under the assumptions made earlier. The relationship between $\bar{h}$ and the flow properties depends on the geometry of the sensor (e.g., wire or sphere) and the flow through empirical heat-transfer correlations.

a. Platinum wire

A wire sensor is assumed to have a cylindrical shape with a diameter d and an infinite length. With those conditions (6) becomes

$$\tau_s = \frac{\rho_s c_s d^2}{4k_f \mathrm{Nu}}, \tag{7}$$

where

$$\mathrm{Nu} = \frac{\bar{h}d}{k_f} \tag{8}$$

is the Nusselt number and k_f is the heat conductivity of the air evaluated at the film temperature. For a long cylinder normal to an airstream for the Reynolds-number range 0.02–44 (the range that encompasses the wire diameters and estimated airspeed in the housings), Collis and Williams (1959) found

$$\mathrm{Nu} = (0.24 + 0.56\,\mathrm{Re}^{0.45})\left(\frac{T_f}{T_\infty}\right)^{0.17}, \tag{9}$$

where

$$\mathrm{Re} = \frac{U_\infty d}{\nu_\infty}. \tag{10}$$

In (9) and (10) Re is the Reynolds number, U_∞ is the free-stream air velocity, ν_∞ is the kinematic viscosity of the air, and T_f is the mean film temperature. The velocity vector is assumed to be normal to the wire. If not, we assume that for an infinitely long wire, the free-stream effective cooling velocity U_e is given by the "cosine law," $U_e = U_\infty \cos\alpha$, where α is the angle between the airspeed velocity vector and the normal to the cylinder axis.

For the NCAR K probe, Spyers-Duran and Baumgardner (1983) indicated that the air flows past the sensor wire at approximately 30% of the true airspeed. There are no data for the flow reduction in the Rosemount 102E4AL, and we assumed a 30% reduction also. Following these assumptions and using (7) for a 25-μm-diameter platinum wire and for a true airspeed $U_\infty = 58\ \mathrm{m\ s^{-1}}$, the value of τ_s was found to be 0.0063 s. This value is 2.5 times smaller than that determined by the manufacturer from wind-tunnel tests, $\tau_s = 0.016$ s. All of the other values listed in Table 1 and determined from in-flight tests are much higher.

The last two examples of Table 1 are results from an experiment by Spyers-Duran and Baumgardner (1983), where two NCAR K probes with $d = 12.5$ and $d = 25$ μm were flown. The difference between the two measured values of τ_s was only about 11%, and both were considerably higher than predicted by (7). For a doubling of the wire diameter and for $U_\infty = 58\ \mathrm{m\ s^{-1}}$, (7) and (9) predict that the time constant is expected to vary as $d^{1.6}$, also found by LaRue et al. (1975). If we apply this law to the NCAR K probe and assume that the value of τ_s for the thicker wire measured by Spyers-Duran and Baumgardner is correct, then the value of τ_s for the 12.5-μm-diameter wire should be about 0.013 s. This would result in a time-constant difference of 200% instead of the measured 11%. This inconsistency may be explained in part by the design of the NCAR K probe. Figure 1c reveals that the wire is aligned almost parallel to the flow direction, whereas in the Rosemount sensor (Fig. 1a), it is wound perpendicular to the average direction of the flow. The parallel configuration reduces the effective cooling velocity considerably, and the expression of the Nusselt number given in (9) is no longer applicable. Therefore, the analysis presented is not particularly applicable for the NCAR K probe, and an expression of Nu for a cylinder parallel to the flow would more be appropriate in describing the heat transfer in this probe.

b. Thermistor

The thermistor bead used in the modified Rosemount sensor is approximately spherical in shape with a nominal diameter of 127 μm. Thus, the expression of the time constant derived from (6) is

$$\tau_s = \frac{\rho_s c_s d^2}{6k_f \mathrm{Nu}}. \tag{11}$$

For a flow past a single sphere and for Re up to 10^5 and $10 < \mathrm{Nu} < 40$, Kramers (1946) found that the following expression of the Nusselt number was verified to within ±10%:

$$\mathrm{Nu} = 2 + 1.3\,\mathrm{Pr}^{0.15} + 0.66\,\mathrm{Pr}^{0.31}\,\mathrm{Re}^{0.5}, \tag{12}$$

where Re is the Reynolds number based on the diameter of the sphere (Re = 186 for the thermistor bead

in our flight conditions) and Pr is the Prandtl number of the free-stream air.

By neglecting heat conduction to the thermistor's support wires and introducing (12) into (11), the calculated value of τ_s was found equal to 0.031 s. The sensor's relative frequency response at −3 dB, $f_{3\,\mathrm{dB}}$, as defined by La Rue et al., can be expressed as

$$f_{3\,\mathrm{dB}} = \frac{1}{2\pi\tau_s}. \tag{13}$$

This gives $f_{3\,\mathrm{dB}} = 5.0$ Hz for the modified Rosemount probe. The experimental value of $f_{3\,\mathrm{dB}}$ deduced from the thermistor power spectra (shown later) is approximately 4 Hz and compares well with the calculated value.

c. *Sensor supports and housing*

The results of Rodi and Spyers-Duran (1971), Lenschow (1972), McCarthy (1973), and Paranthoen et al. (1982) suggest that the response of temperature-sensor wires in probes such as the Rosemount cannot be described adequately by a single-time-constant expression as in (5). They proposed instead a model with a second time constant τ_h that accounts for the additional thermal effects. The nondimensional temperature–time response of the sensor, Θ, is then a two-term exponential expression:

$$\Theta(t) = A_s e^{-t/\tau_s} + A_h e^{-t/\tau_h}. \tag{14}$$

The two constants A_s and A_h must satisfy $A_s + A_h = 1$ to meet the boundary conditions. Values for A_s are listed in Table 1 along with the two time constants τ_s and τ_h.

4. Data

The present data were obtained on the NCAR King Air, which flew approximately 120 h in the Shelf Mixed Layer Experiment (SMILE) off of the west coast of northern California (Enriquez and Friehe 1991). Most of the research flights were conducted at low levels in the marine boundary layer at altitudes of 30 m. Occasional soundings were made to about 1200 m. All temperature sensors remained intact for the duration of the program.

a. *Sea-salt contamination*

A problem with sea-salt contamination on the Rosemount and NCAR temperature sensors was observed for some of the flights, which complicated the analysis slightly. It is well known (Schmitt et al. 1978) that sea-salt aerosols on a temperature sensor produce extra high-frequency spectral energy, due to additional temperature increases and decreases above those of the ambient airstream. These extra fluctuations are due to temperature changes associated with latent heating and cooling in the ambient airstream. This effect has been previously observed on research aircraft operating over the ocean (LeMone and Pennell 1980; Hartmann et al. 1990). Here we present data for which the contamination is minimal, as determined by inspection of the temperature–time series. (Salt-contamination characteristics were not observed for the modified Rosemount sensor with the thermistor. It is not clear at this time whether this is due to the thermistor being new, and therefore starting out clean, or if slight subtleties in the internal flow prevent salt aerosols from accumulating on the bead, or if the small cross-sectional area of the bead simply reduces the probability that the bead becomes contaminated.) It should be noted that the Rosemount platinum element used had flown an unknown number of hours without cleaning and may have been contaminated with various particles. The sensing elements in the Rosemount housings were not washed off during the 120-h SMILE program, whereas the wire in the NCAR K probe was. From the flight data, data records free of sea-salt contamination were selected for transient response and spectral analysis. In the following, ATB will refer to the standard Rosemount sensor, ATKP to the NCAR K probe, and ATFR to the modified Rosemount sensor, per NCAR nomenclature.

b. *Transient*

To examine the transient responses of the three temperature sensors, a vertical sounding through a fairly sharp inversion of approximately 3°C in clear air was chosen. The time series of the sounding is shown in Fig. 2a. The absolute temperatures do not agree, with differences between ATB and ATFR of 0.2°C, and ATB and ATKP of 1°C. In order to compare the responses to the sharp transient at about 200 s and other features, an ad hoc procedure was used to adjust ATFR and ATKP with ATB as the reference. For approximately 30 min before the sounding, the aircraft was flying at constant airspeed in the marine surface layer at 30 m where the air temperature was uniform within 1°C. Therefore it was assumed both that the probe housings and sensor supports were nearly isothermal and that all large transients had decayed. Another nearly isothermal period occurs from 260 to 320 s. Also, except for the main inversion, the heating and cooling rates are reasonably slow, approximately 0.003°C s^{-1}. Our ad hoc procedure was to adjust ATFR and ATKP until they matched ATB (in both dc level and fluctuations) in the isothermal regions. Following this approach, it was found for this flight that the gain of ATFR had to be increased by 2.3% and that ATKP had to be shifted by −1.13°C. The results are shown in Fig. 2b. The match of ATFR and ATB in the isothermal and slow transient regions is very good; the fit of ATKP is good for the first 180 s, but does not fit as well after that. The reason for this inconsistent response is not known.

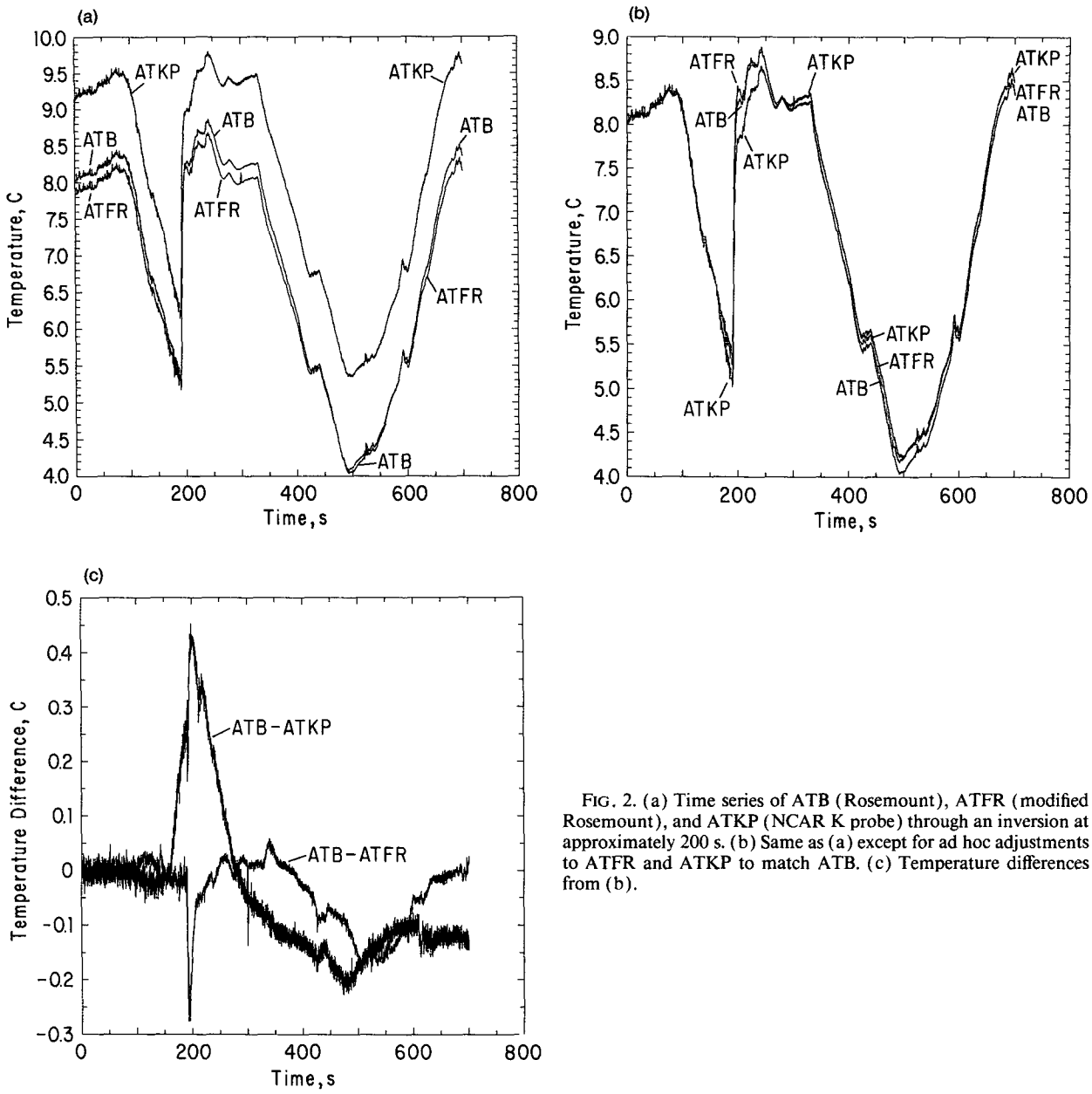

FIG. 2. (a) Time series of ATB (Rosemount), ATFR (modified Rosemount), and ATKP (NCAR K probe) through an inversion at approximately 200 s. (b) Same as (a) except for ad hoc adjustments to ATFR and ATKP to match ATB. (c) Temperature differences from (b).

From Fig. 2b, it is apparent that each sensor has a different response to the inversion transient. The ATKP response in particular lags the change, and also some fine structure at 200 s is not sensed. ATFR appears to sense the fine structure at 200 s slightly better than ATB; that is, more of a temperature increase is measured. These differences are shown in more detail in Fig. 2c, where the differences between ATB and the adjusted ATFR and ATKP signals are shown. The main effect, as noted earlier, is at the inversion. The difference using ATKP is particularly large. The ATB–ATFR signal exhibits a difference of about −0.3°C at the inversion.

From the transient test, it appears that each probe has a different second time constant τ_h. ATB lags ATFR in the sharp rise in temperature at 200 s, probably due to the mica wire supports and possibly other parts remaining cold for about 10–20 s. The converse response in ATB is shown at about 425 s, where the linear cooling is interrupted by a slight rise in temperature. ATB does not heat up as rapidly as ATFR. A similar phenomenon occurs at about 500 s. During the long temperature rise from 500 to 700 s, the two temperatures ATB and ATFR become equal, as presumably the mica support temperature adjusts.

The behavior of the NCAR K probe is less clear. It

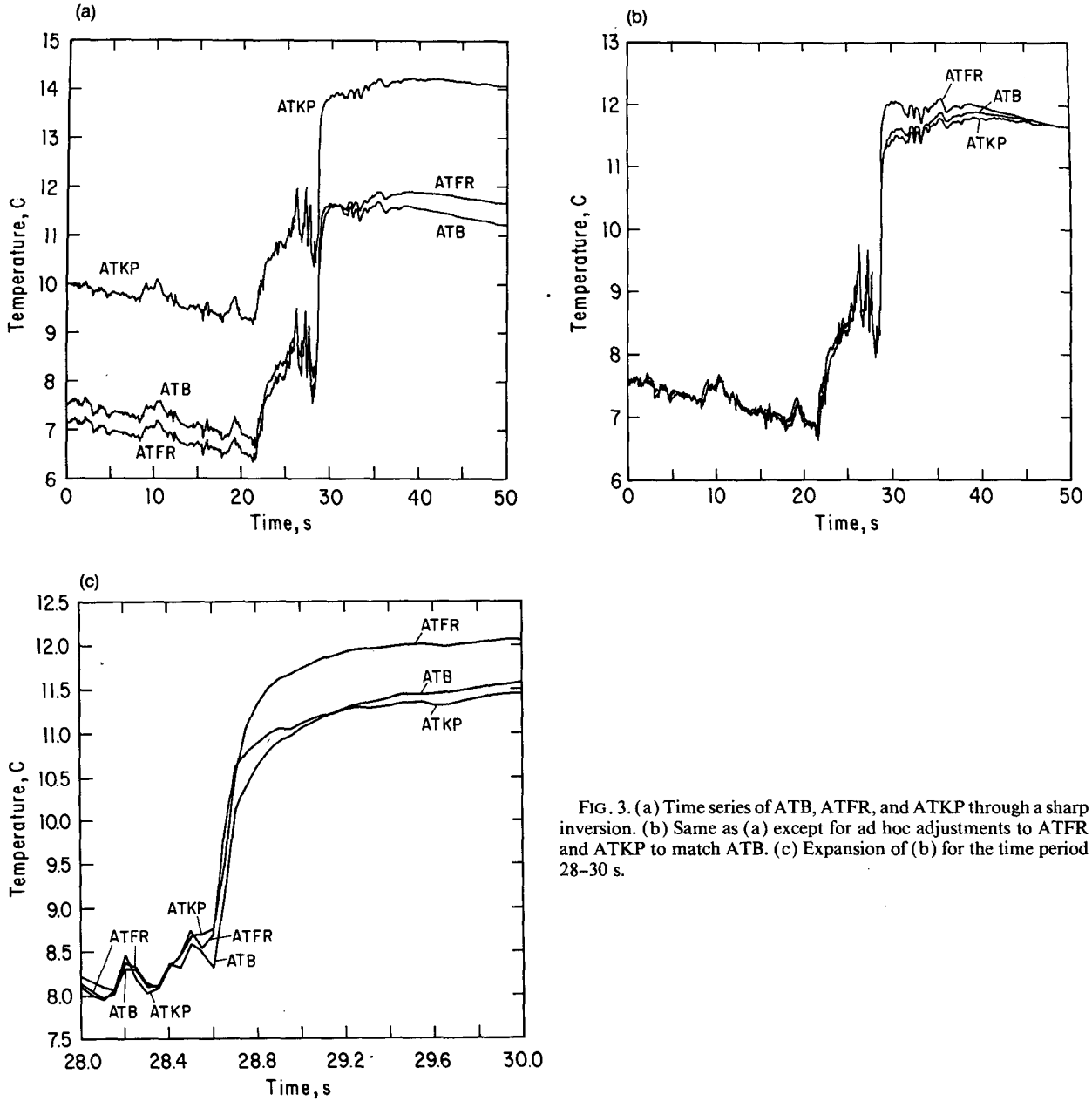

FIG. 3. (a) Time series of ATB, ATFR, and ATKP through a sharp inversion. (b) Same as (a) except for ad hoc adjustments to ATFR and ATKP to match ATB. (c) Expansion of (b) for the time period 28–30 s.

initially tracks ATB and ATFR to about 170 s. Before the inversion it undershoots ATB and ATFR. As noted above, the response at the inversion is particularly poor. A possible explanation for part of the observed response is the influence of the large plastic streamlined body ahead of the sensing wires that is used to separate out cloud water and particles. The air reaching the sensing wires passes over this body, and some heat exchange can occur when the body is at a different temperature than the airstream. Given the large mass of the body, the time constant associated with it should be very large, so that it is always lagging the true temperature changes in a field like that of Fig. 2b after the long-time immersion in the boundary layer. It is not clear, however, that this explains the undershoot before the inversion at 180 s.

c. *Time-constant measurements*

One technique used to estimate the time constants of a temperature sensor consists of fitting its transient response to a temperature step change to the expression given by (14), and thus deducing the values of both housing- and sensing-element time constants. The use of this technique requires data from the three temperature probes through a sharp inversion. The sharper

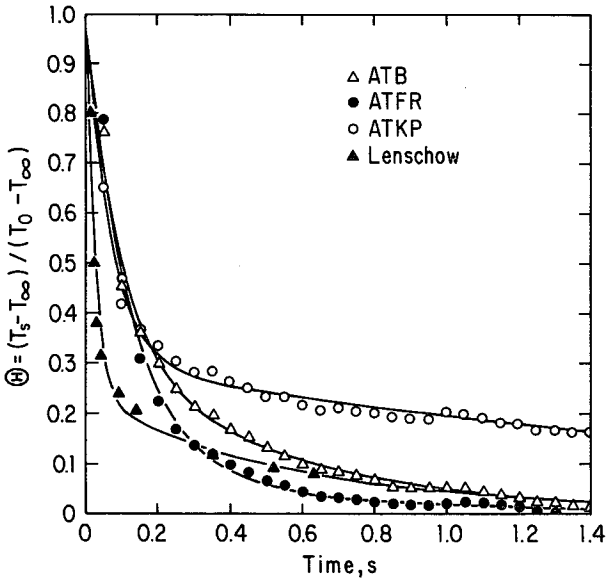

FIG. 4. Normalized temperature response for the data of Fig. 3c and its least-squares-fit curve (solid line): △, ATB, $0.65e^{-t/0.09} + 0.35e^{-t/0.5}$ (error = 0.017); ○, ATKP, $0.70e^{-t/0.07} + 0.30e^{-t/2.3}$ (error = 0.012); ●, ATFR, $0.91e^{-t/0.125} + 0.089e^{-t/0.62}$ (error = 0.020); ▲, Rosemount 102E4AL (Lenschow 1972), $0.77e^{-t/0.025} + 0.23e^{-t/0.59}$ (error = 0.038).

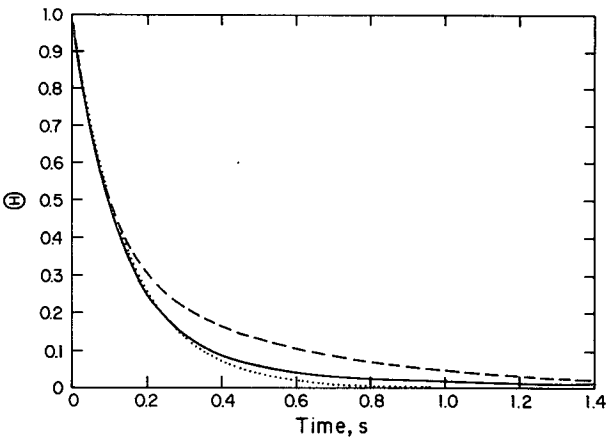

FIG. 5. Response of two- and single-time-constant temperature model to a step change: solid line, modified Rosemount; broken line, standard Rosemount; dotted line, modified Rosemount ($e^{-t/0.148}$).

the inversion, the better its approximation to an ideal step change as assumed in the analysis.

A vertical sounding through an inversion gradient of approximately 20°C s^{-1} was found in the recorded time series and is shown in Fig. 3a before any gain or offset adjustments to ATFR and ATKP were made. To correct the offsets between the three time series, the same ad hoc procedure described in the previous section was followed. It was necessary for this flight to add 0.425°C to ATFR and deduct 2.4°C from ATKP in order to adjust them to the reference probe ATB. The adjusted signals are shown in Fig. 3b where it can be seen that the time responses are similar to those shown in Fig. 2, namely, ATFR leads, followed by ATB and ATKP.

Figure 3c is a close-up of the inversion feature. At t = 28.6 s, the values of the temperatures indicated by ATFR and ATKP are, respectively, 0.5°C and 0.4°C higher than ATB. In order to consider this point as the start of the "step change" and to normalize the temperatures for (14), ATFR and ATKP were reduced by 0.5°C and 0.4°C, respectively. The nondimensional temperatures Θ were calculated from these corrected signals for the time span 28.6–30.0 s. Here T_0 refers to the value given by ATB at t = 28.6 s, and T_∞ to the maximum value reached by ATFR in the plateau immediately after the inversion. A least-squares fitting method was used to find the constants in the two-term exponential expressions of (14) for the data of Fig. 3c. The experimental nondimensional temperatures and best-fit curves are plotted in Fig. 4 for each of the temperature probes. Overall, ATFR has the best transient response. ATKP displays a very fast initial response, but it is considerably slower at long times. The response of ATB is intermediate between those of ATFR and ATKP. The results obtained by Lenschow (1972) for a Rosemount probe are also plotted in Fig. 4. The value of τ_s that he found (0.02 s) is much smaller than the present value of 0.09 s. This is probably due to the fact that the in situ "step change" in temperature used in this study is not a perfect step change, whereas Lenschow produced an instantaneous step change by switching on an electric heating current applied to the wire. The values of τ_s, τ_h, A_s, and A_h obtained for the three probes are listed in Table 2.

To further examine the effects of a two-time-constant stant response on measured temperature signals, we consider the time derivative $d\Theta/dt$ and time integral $\mathcal{A}$ of the normalized temperature Θ from (14):

TABLE 2. Measured parameters of the probes used in the present study.

Sensor	U_∞ (m s^{-1})	d (μm)	Re	A_s	τ_s (s)	τ_h (s)
Rosemount 102E4AL	70.0	25	36.5	0.65	0.09	0.5
NCAR K probe	70.0	25	36.5	0.70	0.07	2.3
Thermistor	70.0	127	186	0.91	0.125	0.62

TABLE 3. Effects of sensing element and housing on time response.

Sensor	$\mathcal{A}$ (s)	$\mathscr{H}$ (s)	$A_s\tau_s$ (s)	H_{ef} (s)	$100A_s\tau_s/\mathcal{A}$	$100H_{ef}/\mathcal{A}$	$\mathscr{S}$ (s^{-1})
Rosemount 102E4AL	0.223	0.175	0.058	0.164	26.3	73.7	7.24
NCAR K probe	0.363	0.69	0.049	0.314	13.48	86.5	10.0
Thermistor	0.163	0.055	0.114	0.049	69.7	30.3	7.29

$$\frac{d\Theta}{dt} = -\frac{A_s}{\tau_s}e^{-t/\tau_s} - \frac{A_h}{\tau_h}e^{-t/\tau_h} \tag{15}$$

$$\mathcal{A} = \int_{t_1}^{t_2}\Theta dt = A_s\tau_s(e^{-t_1/\tau_s} - e^{-t_2/\tau_s}) + A_h\tau_h(e^{-t_1/\tau_h} - e^{-t_2/\tau_h}), \tag{16}$$

where t_1 and t_2 are integration times. The derivative response is essentially set by the first term in (15), since typically $A_s/\tau_s \gg A_h/\tau_h$. The integral response is determined by $A_h\tau_h$ in (16), since it is usually greater than $A_s\tau_s$.

Therefore, we define two sensor parameters as

$$\mathscr{S} = \frac{A_s}{\tau_s}, \tag{17}$$

and

$$\mathscr{H} = A_h\tau_h. \tag{18}$$

An ideal sensor would have $\mathscr{S} \to \infty$ and $\mathscr{H} \to 0$. Figure 5 shows the least-squares-fit curves representing Θ versus t for the standard and modified Rosemount probes for the response to a step change. The area $\mathcal{A}$ would be zero for an ideal sensor; the modified sensor does show improvement over the standard Rosemount. For the 1.4 s of data of Fig. 5, $t_1 = 0$ and $t_2 = 1.4$ s, and since $e^{-1.4/\tau_s}$ is small, $\mathcal{A}$ is given approximately by

$$\mathcal{A} \approx A_s\tau_s + H_{ef}, \tag{19}$$

where

$$H_{ef} = \mathscr{H}(1 - e^{1.4/\tau_h}). \tag{20}$$

The first term in (19) is the contribution of the sensing element to $\mathcal{A}$; the second is due to the supports and housing. Values of $\mathcal{A}$, $\mathscr{H}$, H_{ef}, etc., are presented in Table 3 for the three sensors. The percentages of $\mathcal{A}$ due to the supports and housing are 86.5%, 73.7%, and 30.3% for the NCAR K probe, standard Rosemount, and thermistor, respectively. Thus, the thermistor sensor decreases the housing and support term by about a factor of 2; $\mathscr{H}$ decreased from 0.175 to 0.055 s as shown in Table 3.

The derivative response is shown in Figs. 6a and 6b for the standard and the modified Rosemount probes, respectively. The responses are essentially the same. While the 25-μm-diameter platinum wire element itself responds faster than the $d = 127$ μm thermistor bead, the $\mathscr{S}$ terms are essentially identical, as shown in Table 3.

Since the housing and support term is smaller for the modified Rosemount than for the other probes, its response can be approximated by a single-time-constant expression of $\Theta = e^{-t/0.148}$ (t in seconds) with a deviation[4] of only 0.026 in Θ compared to the data in Fig. 4. This is also shown in Fig. 5.

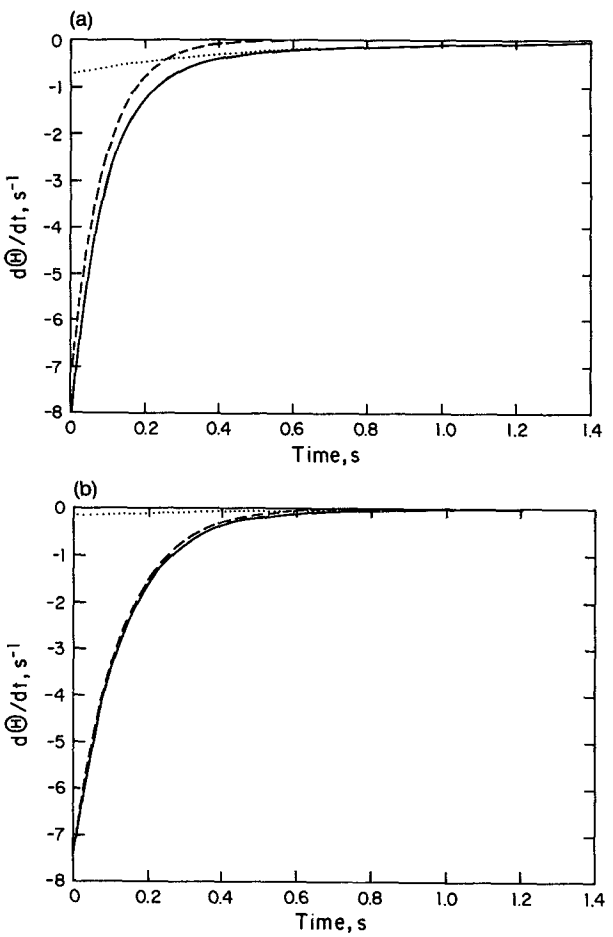

FIG. 6. (a) Derivative of the normalized temperature for the standard Rosemount: solid line, $d\Theta/dt$; broken line, $-\mathscr{S}e^{-t/\tau_s}$; dotted line, $-(A_h/\tau_h)e^{-t/\tau_h}$. (b) Derivative of the normalized temperature for the modified Rosemount: solid line, $d\Theta/dt$; broken line, $-\mathscr{S}e^{-t/\tau_s}$; dotted line, $-(A_h/\tau_h)e^{-t/\tau_h}$.

[4] The deviation, also called error or residual, is defined in the least-squares sense as $[\sum_{i=1}^{N}(\Theta_{mi} - \Theta_{ei})^2/N]^{0.5}$, where m and e refer to the model and the experiment, respectively.

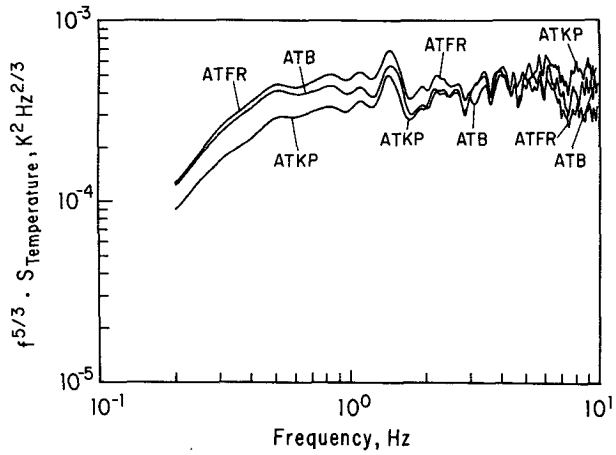

FIG. 7. Power spectra ($\times f^{5/3}$) for ATB, ATFR, and ATKP.

Our results confirm that ATKP, with $\mathcal{S} = 10.0\ s^{-1}$, has the fastest short-time response, as was found earlier by Spyers-Duran and Baumgardner (1983). They found that the NCAR K probe does not have a secondary time constant ($A_h = 0.0$; thus $\mathscr{K} = 0.0$), while the present study shows that this sensor has the largest second time constant and housing factor ($\tau_h = 2.3$ s, $\mathscr{K} = 0.69$ s).

d. Spectral analysis

Spectral analysis was performed on approximately 8 min of data obtained in the marine boundary layer at 30-m altitude for which the previous ad hoc adjustments were not applied. The spectra S_{ATB}, S_{ATFR}, and S_{ATKP} for ATB, ATFR, and ATKP, respectively, are shown in Fig. 7. In order to readily identify the scalar inertial–convective subrange (Tennekes and Lumley 1972), the spectra have been multiplied by $f^{5/3}$, which plots as a straight horizontal line for the subrange. For all three signals a section corresponding to this inertial subrange can be observed at higher frequencies. There is some evidence for slightly more spectral variance between 0.1 and 4 Hz with ATFR compared to ATB. ATKP displays clearly less spectral energy than the two others in this frequency range. This is shown in more detail in Fig. 8, where the power spectral ratios S_{ATFR}/S_{ATB}, S_{ATKP}/S_{ATB}, and S_{ATKP}/S_{ATFR} are plotted versus frequency. The spectral energy of ATKP is 20%–35% less than that of ATB for the frequencies up to 2 Hz; for higher frequencies it is approximately 30% greater than that for the Rosemount. The ratio S_{ATKP}/S_{ATFR} increases almost steadily from 0.6 at $f \sim 0.4$ Hz to 1.8 at $f \sim 8$ Hz. It can be inferred from the variations of these three ratios that ATKP has better frequency response than the two other probes at higher frequencies, which confirms the results found in the previous section on time response.

Additional evidence showing that ATKP has superior high-frequency response to both ATB and ATFR is shown in Fig. 9a, where the phase shifts between the three signals obtained from spectral analysis are plotted. The phase of ATKP leads ATB with 7° and ATFR with 14° in the frequency range 4–10 Hz. The phase of ATFR leads ATB slightly to about 1 Hz, whereafter it lags, consistent with the −3-dB frequency response of the thermistor of about 4 Hz. The three phase shifts verify the relation $\phi_{ATKP,ATB} = \phi_{ATKP,ATFR} + \phi_{ATFR,ATB}$ for all frequencies.

Measurements of the coherence, γ, between the three signals are plotted in Fig. 9b. These curves show that the signals are well correlated and that the phase data are meaningful: γ remains greater than 0.8 up to $f \sim 4$ Hz for ATKP and ATB, up to $f \sim 6$ Hz for ATFR and ATB, and up to approximately 7 Hz for ATKP and ATFR. These last two signals seem to be more coherent, which may be due in part to the fact that they were installed close to each other on the same side of the radome, whereas the ATB probe was mounted on the other side.

As mentioned in the Introduction, an important application of aircraft temperature sensors is the measurement of sensible heat flux. The vertical turbulent flux of heat is

$$H = \rho c_p \overline{w\theta}, \tag{21}$$

where ρ is the air density, c_p specific heat at constant pressure, w and θ the vertical velocity and temperature fluctuations, respectively, and the overbar denotes a time average. Because the covariance $\overline{w\theta}$ is equal to the integral of the cospectrum between w and θ over frequency, calculating the heat flux is equivalent to estimating the area under the cospectrum. Heat-flux cospectra are presented in Fig. 10 for all three probes. Most of the contribution to the heat flux for the present

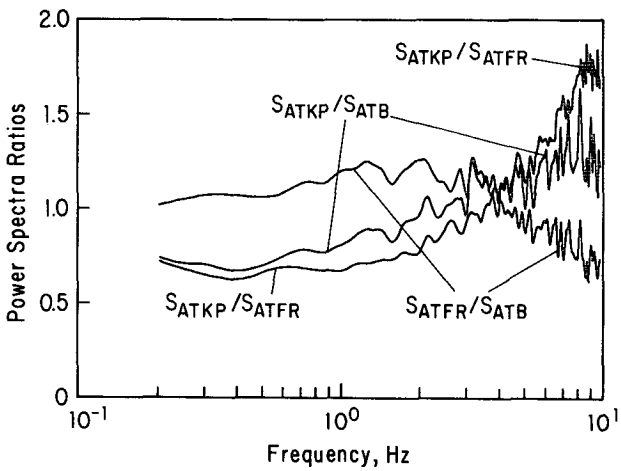

FIG. 8. Ratios of power spectra of Fig. 5.

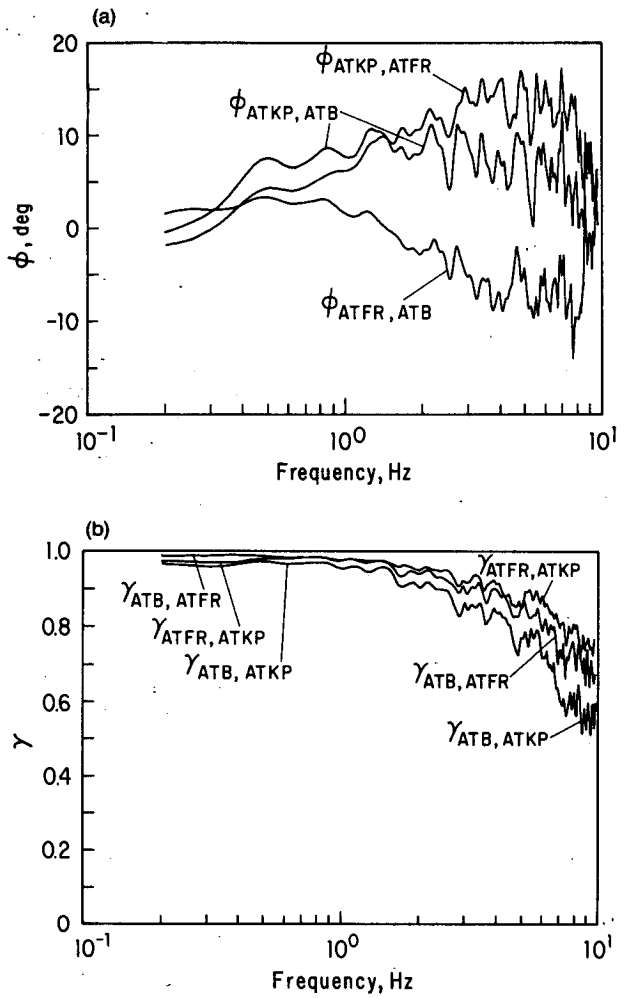

FIG. 9. (a) Phase between ATFR, ATB; ATKP, ATB; ATKP, ATFR. Positive phase angle between X and Y means that X leads Y. (b) Coherence between ATFR, ATB; ATKP, ATB; ATKP, ATFR.

data occurs at low frequencies ($f \leq 6$ Hz). The heat flux measured with ATFR is 3.4% and 18% greater than those with ATB and ATKP, respectively.

5. Discussion

These in situ comparisons illustrate some of the characteristics of fast-response aircraft temperature sensors. The two-time-constant response of the standard Rosemount was verified. The value of τ_h of 0.5 s obtained in the present work is intermediate between previous values 1.15 (McCarthy 1973a) and 0.17 s (Spyers-Duran and Baumgardner 1983). This second time constant was reduced by replacing the platinum wire–bobbin assembly with a small thermistor bead. The results with the modified Rosemount sensor therefore indicate that the small l/d of the platinum wire suspended between the mica supports is a major cause of the second time constant, following the analysis of Lenschow (1972) and Paranthoen et al. (1982).

The NCAR K probe with very large l/d wire elements (~2000) did exhibit superior high-frequency response, but there were peculiarities and inconsistencies in the transient response through sharp inversions that are not understood. We suggest that the ellipsoidal plastic body placed upstream of the wire may have sufficient heat capacity to influence the wire temperature, although this cannot explain all of the observed responses of the K probe.

The theoretical analysis of the time responses of the wires and thermistor agreed reasonably well with the observed values, given the uncertainty of estimating the flow velocity inside the Rosemount housing. Since the wire element in the K probe lies approximately parallel to the airstream, rather than in the usual perpendicular direction, the present analysis is not particularly applicable.

6. Conclusions

The present results suggest that an overall improvement in the response of fast-response aircraft temperature sensors can be obtained by replacing the two-time-constant wire element in the standard Rosemount probe with a small thermistor. The longer time constant is reduced with this modification, which means that sharp features such as inversions are more accurately measured. The limitation is the response of the thermistor bead itself. The smallest available bead has a −3-dB frequency of about 4 Hz. In principle, the time-series data from the standard Rosemount probe can be corrected both for the longer time constant and the shorter one due to the wire itself, as Ritter et al. have done, but very accurate values for τ_s, τ_h, and A_s are required. In view of the wide range of values obtained

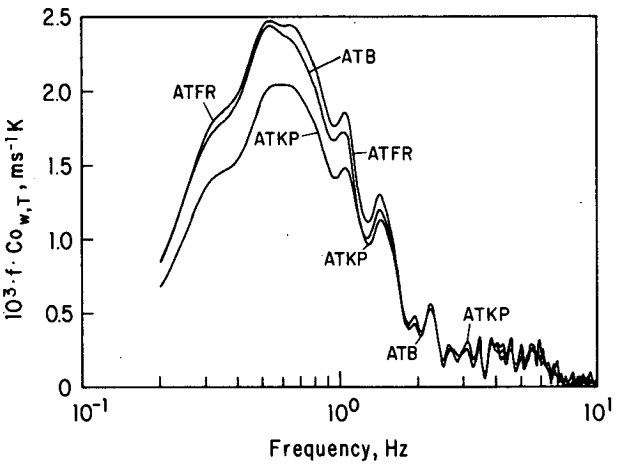

FIG. 10. Cospectra (times frequency) of w and ATB, ATFR, and ATKP.

in this and previous studies for the parameters, it therefore seems better to avoid the longer time constant altogether.

It would seem possible to correct for the response of the thermistor bead itself, since its characteristics appear to be reasonably well known. The uncompensated upper limit of about 4–5 Hz is just adequate for eddy-correlation heat-flux measurements. We are planning test flights with a dual TSI probe, where the 127-μm thermistor can be flown simultaneously with a 1.2-μm platinum wire (l/d = 1000). This extremely thin sensing element will have a response to at least 1 KHz. The test data should provide an algorithm for compensation of the thermistor to at least 25 Hz, adequate for flux measurements, resolution of the temperature inertial subrange, and measurements of extremely sharp inversions.

Finally, we note that temperature calibration is a continuing problem. We arbitrarily used the Rosemount probe (and its amplifier) as the standard. The thermistor was calibrated in a temperature bath of deionized water, but the dc amplifier used only low-quality operational amplifiers whose lack of stability and narrow environmental temperature range may have accounted for some of the shifts observed through the flights. We do not have an explanation for the larger offset of the NCAR K probe.

Acknowledgments. This work was supported by the Office of Naval Research Marine Meteorology Program and the Division of Ocean Sciences of the National Science Foundation. We would like to thank the Research Aviation Facility of the National Center for Atmospheric Research for their support. Jim Perez fabricated the sensor, and Todd Sutton built the electronics. We also thank Don Lenschow and the reviewers for their valuable comments.

REFERENCES

Acheson, D. T., 1973: Comments on "A method for correcting airborne temperature data for sensor response time." *J. Appl. Meteor.*, **12,** 1089–1090.

Brown, E. N., C. A. Friehe, and D. H. Lenschow, 1983: The use of pressure fluctuations on the nose of an aircraft for measuring air motion. *J. Climate Appl. Meteor.*, **22,** 171–180.

Collis, D. C., and M. J. Williams, 1959: Two-dimensional convection from heated wires at low Reynolds numbers. *J. Fluid Mech.*, **6,** 357–384.

Enriquez, A. G., and C. A. Friehe, 1991: Variability of the atmospheric boundary-layer over a coastal shelf in winter during SMILE. Preprints, *Fifth Conf. on Meteorology and Oceanography of the Coastal Zone,* Miami, Amer. Meteor. Soc., 102–107.

Hartmann, J., J. Hacker, and H. Kraus, 1990: Correction of data from a salt-spray contaminated temperature sensor. *Bound.-Layer Meteor.*, **50,** 153–169.

Kramers, H., 1946: Heat transfer from spheres to flowing media. *Physica,* **XII,** No. 2-3, 61–80.

LaRue, J. C., T. Deaton, and C. H. Gibson, 1975: Measurements of high-frequency turbulent temperature. *Rev. Sci. Instrum.*, **46,** 757–764.

Lawson, R. P., 1991: Design and preliminary tests of a new airborne thermometer. Preprints, *Seventh Symp. on Meteorological Observations and Instrumentation,* New Orleans, Amer. Meteor. Soc., 366–371.

LeMone, M. A., and W. T. Pennell, 1980: A comparison of turbulence measurements from aircraft. *J. Appl. Meteor.*, **19,** 1420–1437.

Lenschow, D. H., 1972: The measurements of air velocity and temperature using the NCAR Buffalo aircraft measuring system. NCAR Tech. Note TN/EDD-74, 39 pp.

McCarthy, J., 1973a: A method for correcting airborne temperature data for sensor response time. *J. Appl. Meteor.*, **12,** 211–214.

——, 1973b: Reply. *J. Appl. Meteor.*, **12,** 1090–1091.

Paranthoen, P., C. Petit, and J. C. Lecordier, 1982: The effect of the thermal prong-wire interaction on the response of a cold wire in gaseous flows (air, argon and helium). *J. Fluid Mech.*, **124,** 457–473.

Ritter, J. A., G. L. Smith, and D. R. Cahoon, 1987: The use of a numerical filter to correct airborne temperature measurements for the effects of sensor lag. *Extended Abstracts, Sixth Symp. on Meteorological Observations and Instrumentation,* New Orleans, Amer. Meteor. Soc., 261–264.

Rodi, A. R., and P. A. Spyers-Duran, 1972: Analysis of time response of airborne temperature sensors. *J. Appl. Meteor.*, **11,** 554–556.

Rosemount, 1963: Total temperature sensors. Rosemount Engineering Company Tech. Bulletin No. 7637, 27 pp.

Sandborn, V. A., 1972: *Resistance Temperature Transducers.* Metrology Press, 545 pp.

Schmitt, K. F., C. A. Friehe, and C. H. Gibson, 1978: Humidity sensitivity of atmospheric temperature sensors by salt contamination. *J. Phys. Oceanogr.*, **8,** 151–161.

Spyers-Duran, P., and D. Baumgardner, 1983: In flight estimation of the time response of airborne temperature sensors. Preprints, *Fifth Symp. on Meteorological Observations and Instrumentation,* Toronto, Amer. Meteor. Soc., 352–357.

Tennekes, H., and J. L. Lumley, 1972: *A First Course in Turbulence.* The MIT Press, 300 pp.

Wyngaard, J. C., 1988: The effects of probe-induced flow distortion on atmospheric turbulence measurements: Extension to scalars. *J. Atmos. Sci.*, **45,** 3400–3412.